Retrieval of relevant parameters of natural multilayer systems by means of bio-inspired optimization strategies

Demetrio Macías,[1,*] Ana Luna,[2] Diana Skigin,[2] Marina Inchaussandague,[2] Alexandre Vial,[1] and Daniel Schinca[3]

[1]Institut Charles Delaunay-Laboratoire de Nanotechnologie et d'Instrumentation Optique (ICD-LNIO), UMR CNRS 6279, 12, rue Marie Curie - CS42060, Troyes Cedex F-10004, France

[2]Grupo de Electromagnetismo Aplicado, Departamento de Física, FCEN, Universidad de Buenos Aires, and IFIBA, CONICET, Pabellón 1, Ciudad Universitaria (C1428EHA) Buenos Aires, Argentina

[3]CIOp (CONICET, CIC), cc 124, 1900 La Plata, Árgentina and Área Departamental de Ciencias Básicas, Facultad de Ingeniería, Universidad Nacional de La Plata, La Plata, Argentina

*Corresponding author: demetrio.macias@utt.fr

Received 3 January 2013; revised 26 February 2013; accepted 27 February 2013; posted 5 March 2013 (Doc. ID 182531); published 10 April 2013

Natural photonic structures exhibit remarkable color effects such as metallic appearance and iridescence. A rigorous study of the electromagnetic response of such complex structures requires to accurately determine some of their relevant optical parameters, such as the refractive indices of the materials involved. In this paper, we apply different heuristic optimization strategies to retrieve the real and imaginary parts of the refractive index of the materials comprising natural multilayer systems. Through some examples, we compare the performances of the inversion methods proposed and show that these kinds of algorithms have a great potential as a tool to investigate natural photonic structures. © 2013 Optical Society of America

OCIS codes: (050.5298) Photonic crystals; (050.1755) Computational electromagnetic methods; (170.1420) Biology.

http://dx.doi.org/10.1364/AO.52.002511

1. Introduction

There are two main mechanisms to achieve coloration in the biological world: pigmentary and structural. The former has a chemical origin and is generated by the selective absorption of natural light. The later, also known as structural color, has a physical origin and is generated through the interference, diffraction, or scattering phenomena that arise as a consequence of the interaction between natural light and the microstructures present in the cover tissues of animals and plants. In general, color results from a combination of pigmentary and structural effects [1,2]. Also, when iridescent colors are produced, the hue changes with viewing angle, and the color is very intense and highly saturated [3,4].

In addition to different geometrical features, such as surface-roughness and/or the presence of periodic/aperiodic multiple layers, the refractive indices of the materials involved determine the structural color in biological specimens. Also, most structurally colored biological systems contain absorbing pigments [5], which implies a variation in both the real and the imaginary parts of the refractive index. Therefore, a precise knowledge of these constitutive parameters, i.e., the materials that compose the biological tissues, is essential for the study of this type of system [6]. Recently, a few authors reported different methods to retrieve the complex refractive indices

1559-128X/13/112511-10$15.00/0

of some biological structures. For instance, an effective medium theory has been applied to a multilayer film to determine the anisotropic index of refraction of the cuticle's material of the wings of the butterfly *Morpho Menelaus* [7]. Also, measurements using index-matching techniques have been used to find the refractive index of the cuticle material comprising the microstructure of the *Morpho* butterfly scales [8]. Leertouwer *et al.* used Jamin–Lebedeff interference microscopy to measure the wavelength dependence of the refractive index of butterfly wing scales and bird feathers [9]. Furthermore, the complex refractive indices of the natural multilayer reflector in the beetle *Chrysochroa raja* were found by the application of a known optical characterization technique [10]. In [11], the authors have proposed an iterative procedure, based on Cauchy's and Fresnel's equations, to retrieve the refractive index from experimental data, and Arwin *et al.* used Mueller's matrix ellipsometry data to obtain the equivalent refractive index of the materials that constitute the multilayer cuticle of different beetles [12].

Together with a rigorous experimental technique, Noyes *et al.* [10] employed a recursive fitting algorithm to retrieve the complex refractive index of their biological sample. Nevertheless, neither the operational principles nor issues such as the convergence rate of their approach were discussed. Thus, given the difficulties to experimentally measure the constitutive parameters of natural structures, it seems well worth exploring further the possibilities of inversion strategies such as the one proposed in [10], as they could provide an alternative way not only to determine optical or geometrical parameters of biological samples, but also to characterize and mimick their optical response for specific applications [13]. To this end, in this work we employ an inversion scheme based on heuristic optimization algorithms. These techniques have been extensively and successfully applied for the solution of different approximation problems such as near-field optics microscopy or random rough surfaces profilometry [14,15], the dispersion modeling of the optical constants of metals [16,17], the optimization of plasmonic structures [18,19], or very recently, the optimization of some resonant properties of metallic star-like nanostructures [20,21]. Therefore, heuristic optimization appears as a very good candidate to be applied for the retrieval of relevant parameters of natural microstructures as, for example, the complex refractive indices of multilayer systems like those found in plants [22], spiders [23], and beetles [10,24–28].

This paper is structured as follows: In Section 2 we outline the hybrid approach used to retrieve the parameters of interest and give the theoretical details of the methods employed. Also, we briefly describe the operational principles of the two different bio-inspired techniques to be used in this work: evolution strategies (ES), through their elitist (EL) and nonelitist (NE) variants, and particles swarm optimization (PSO). Section 3 is devoted to illustrate the performance of the retrieval method proposed through some validation and application examples. In particular, we estimate the dielectric constants of the multilayer structure that composes the elytra of the *Ceroglossus suturalis* beetle (Coleoptera order) from experimental reflectance measurements. Finally, concluding remarks are provided in Section 4.

2. Theoretical Approach

The essential idea of the inversion method proposed in this work is sketched in Fig. 1, which shows the basic stages to obtain an optical signal, e.g., reflectance spectrum, from a biological sample. The hatched pink arrows illustrate the experimental measurement of the optical signal. Also, the top-hatched blue arrow shows the importance of a precise characterization of the sample's microstructure, through different microscopy techniques, on the establishment of an adequate geometrical model. Once this is done, a rigorous electromagnetic method (analytical or numerical) is employed to calculate the optical signal for different geometrical and constitutive parameters of the natural system. As indicated by the solid blue arrow, this should lead to a theoretical curve that, in principle, must agree with the experimental one. What has been just described corresponds to the solution of the direct or forward problem. However, as indicated with the solid red arrow, in this contribution we aim at retrieving the constitutive parameters of the natural system from the experimental/theoretical reflectance information. Then, as shown by the solid blue arrow, we include an inversion loop that couples the forward electromagnetic model with a particular heuristic optimization technique.

A. Heuristic Optimization: Evolution Strategies and Particles Swarm Optimization

As stated previously, any forward electromagnetic method can be used to compute the reflected and transmitted fields. Nevertheless, the relationship between this information and the geometrical and material features of the microstructure is not a trivial one. Consequently, the establishment of an inversion scheme directly from the forward electromagnetic model is a formidable task itself. This situation could be overcome through some simplifying assumptions that would lead to an analytical model. However, the validity of this approach would be limited only to a few specific cases. An alternative way to solve this kind of inverse problem is to reformulate it in terms of Approximation Theory. For this, we define the functional

$$f(\mathbf{p}^T) = \|I^{\exp}(\lambda) - I^{\text{the}}(\lambda|\mathbf{p}^T)\|_2^2, \tag{1}$$

where $\|\|_2$ is the Euclidean Norm, the components of vector $\mathbf{p}^T$ are the parameters to be retrieved, and $I^{\exp}(\lambda)$ and $I^{\text{the}}(\lambda|\mathbf{p}^T)$, respectively, represent the experimentally measured and numerically generated spectra. At least in principle, the minimization of Eq. (1) should lead, if the solution is unique, to a

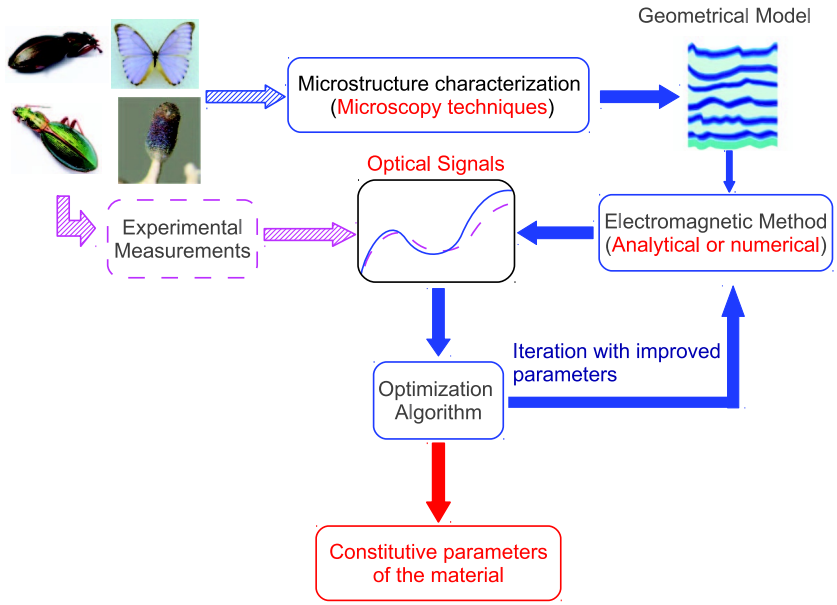

Fig. 1. Scheme of the inversion procedure proposed to retrieve the relevant parameters of biological microstructures.

set of parameters that reproduce the experimental optical signal. In the examples to be treated, these parameters are the dielectric constants, real and imaginary parts, of the multilayer structure studied. However, this choice is not restrictive and could be the thicknesses of the layers or any other magnitude of interest.

1. *Evolution Strategies*

We have found in previous contributions that ES, a variant of the so-called evolutionary algorithms, are a suitable and versatile tool for the optimization of functionals similar to that defined in Eq. (1) [14,15]. Since we will employ these techniques in the present work, we consider it convenient to succinctly describe their operational principles in the following paragraphs. For a more detailed depiction, we refer the interested reader to the excellent work of Beyer [29].

The first step prior to the beginning of the optimization process is the random generation of an ensemble of vectors $\mathbf{p}^T$ that will conform the initial population $P_\mu^{\langle g\rangle}|_{g=0}$, where μ is the number of elements within the population and g is the associated iteration of the algorithm. A canonical evolutionary optimization algorithm is based on the application, over a defined number of iterations, of two genetic operators with well defined roles. The first is the recombination, which exploits the search space through the exchange of information between ρ different elements of the population. The second operator is the mutation, which is used to explore the search space through the introduction of random variations in the population. The application of these genetic operators over the initial population leads to the generation of a secondary population $P_\lambda^{\langle g\rangle}$ of λ elements. It is at this stage of the evolutionary loop that the link between the physics of the problem studied and the optimization algorithm is established. In the present work, this is done through the minimization of the functional defined in Eq. (1), which can also be interpreted as a measure of the closeness between the reflectance data and those computed with a previously established model. Each element of the secondary population will be evaluated, and only those elements of $P_\lambda^{\langle g\rangle}$ that minimize the Euclidean norm will be retained, through some selection scheme, as part of the population $P_\mu^{\langle g+1\rangle}$ for the next iteration of the evolutionary loop. The procedure is repeated until a defined termination criterion has been achieved. The respective sizes of the initial and the secondary populations, $P_\mu^{\langle g\rangle}$ and $P_\lambda^{\langle g\rangle}$, remain constant throughout the entire search process.

It is convenient to mention that the initial populations can be selected, throughout the evolutionary loop in two different ways: NE $(ES-(\mu/\rho,\lambda))$ and EL $(ES-(\mu/\rho+\lambda))$. The main difference between these two schemes is that the former selects the best elements only from the mutated population. The latter, on the other hand, selects the best elements from an intermediate population generated from the junction of the initial and mutated populations. Consequently, a promising element belonging to the first initial population can survive throughout the entire optimization process. Although this attribute of the EL strategy guarantees a monotonic decrement or increment of the fitness function, it can also make it prone to premature convergence into a local optimum.

2. *Particles Swarm Optimization*

The PSO is a fairly recent heuristic optimization method proposed by Eberhart and Kennedy in the mid-1990s [30]. The underlying biological mechanism of this population-based technique is not related to the evolution of the elements belonging to a population, as is the case for the genetic

algorithms [31] or the ES [32]. Instead, the PSO imitates, throughout its search for the optimum, the social and collaborative behavior of a group of individuals such as, for example, a flock of birds, a school of fish or a swarm of bees, during their quest for eatables. This search for a region of the space potentially rich in food depends on the exchange of information based on both, the common knowledge of the swarm and the individual experience of each of its elements.

Although different variants have been proposed through the years, and excellent works on the theory of the PSO can be found elsewhere [33,34], we will briefly summarize its operational principles in the following paragraphs. For the sake of clarity, we will use the same notation as that for the ES.

The first step prior to the search for the optimum is the random generation of a population of μ particles. Each of them is composed of n variables that, depending on the context of the problem studied, represent the quantities of interest that need to be optimized. Also, these variables are interpreted as the coordinates of each particle in an n-dimensional space.

Once the initial locations and speeds have been generated, the search process starts with the evaluation of the individual fitness *pbest* of each particle in the population. The global optimum of the swarm, *gbest*, is then obtained from the set of optima *pbest* previously computed. This information will then serve to modify the location of the swarm through the operator

$$x_{m,i}^{\langle g+1\rangle} = x_{m,i}^{\langle g\rangle} + \Delta t v_{m,i}, \tag{2}$$

where $m = 1, 2, \ldots, \mu$ and $i = 1, 2, \ldots, n$ represent an element of the swarm and the corresponding variable of interest, respectively. The index g is associated to a specific iteration of the search process. The factor Δt is usually assumed to be one. The speed $v_{m,i}$ is modified through the weighted sum

$$\begin{aligned} v_{m,i} = {} & w v_{m,i} + c_1 U_1 (pbest_{m,i} - x_{m,i}) \\ & + c_2 U_2 (gbest_i - x_{m,i}), \end{aligned} \tag{3}$$

where $0.0 \le U_\alpha \le 1.0$ with $\alpha = 1, 2$ are two uniformly distributed random numbers that will serve to include the unpredictable behavior of the swarm throughout the entire search. The coefficients c_1 and c_2 are two scale factors to respectively determine the influence that the individual fitness (*pbest*) and the global fitness of the swarm (*gbest*) will have on the particle's new speed and location for the next iteration of the search process. The coefficient $0.0 \le w \le 1.0$ is called the *inertia factor* and measures how much the original location of the particle is affected by the personal and global optima *pbest* and *gbest*, respectively. The steps just described are repeated until a previously established stop criterion has been reached. This can be the number of iterations or the convergence of the population to the optimum. It is noteworthy that the size of the population, as is the case for the ES, does not change throughout the entire optimization process.

B. Forward Electromagnetic Solver

In general, different natural microstructures, such as thin films, diffraction gratings, photonic crystals, etc., can be identified as responsible for the color effects. Therefore, depending on the type of structure, the forward electromagnetic model should be chosen. In many biological structures, the iridescent response is clearly governed by the periodic multilayers present in the most external cover tissues. These structures usually exhibit imperfections, such as surface roughness and nonuniform thickness, and their distribution is not perfectly periodic. However, as a first approach, a periodic planar multilayer appears as a suitable model to represent such system, as schematically shown in Fig. 2. The 4×4 transfer matrix method for one-dimensional multilayer systems is used to find the solution of the direct problem, i.e., to compute the scattered electromagnetic response given all the parameters of the structure. This method consists in combining Maxwell equations with the corresponding constitutive relations to obtain a differential system for the unknown electric and magnetic field components in each layer. For structures with translational invariance and assuming plane wave illumination, this system can be reduced to a 4×4 differential system, whose unknowns are the tangential components of the electric and the magnetic fields. Imposing the boundary conditions at each interface, one ends with a 4×4 matrix system for the unknown amplitudes outside the structure, i.e., transmitted and reflected. It is important to remark that this method is suitable for dealing with periodic and nonperiodic multilayer structures, and can also handle general media described by arbitrary permittivity and permeability tensors. The details of the method can be found in [35].

3. Results

At this stage, some examples are convenient to illustrate the possibilities of the inversion scheme just proposed. To validate our approach and assess

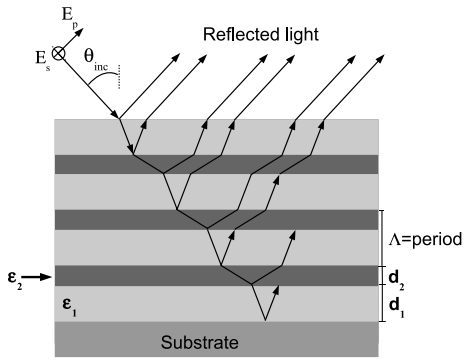

Fig. 2. Scheme of the planar periodic multilayer model.

its performance, we retrieve the dielectric constants of a multilayer system from numerically generated reflectance spectra. Then, in a second example, we look for the relevant parameters from experimentally measured spectra. The results are discussed in the last part of this section.

A. Validation Example

In this first example, we numerically generate, by means of the 4×4 method, the target reflectance spectrum from where we aim at retrieving the complex values of ϵ_1 and ϵ_2. The incident field is assumed to be a *p*- or *s*-polarized plane wave. Also, we consider a periodic bilayer structure that comprises nine periods, with layers of thicknesses $d_1 = 60$ nm and $d_2 = 100$ nm (see Fig. 2). The respective dielectric constants of these layers are $\epsilon_1 = 2.3829 + i0.434$ and $\epsilon_2 = 2.8215 + i0.1008$, as reported by Noyes *et al.* for the Buprestid beetle [10]. The incidence medium is air and the dielectric constant of the substrate was taken to be $(\epsilon_1 + \epsilon_2)/2$, as reported for other beetles' structures [28].

Concerning the ES, throughout this numerical experiment we set the sizes of the initial and the secondary populations to $\mu = 14$ and $\lambda = 100$, respectively. Furthermore, we fixed the number of elements to be recombined to $\rho = 2$. The number of generations in the evolutionary loop was set to $g = 100$ and it provided the termination criterion. In this example, each element of the population was a set of randomly generated values of ϵ_1 and ϵ_2, this means that we will look for four unknowns: the real and imaginary parts of each dielectric constant. Thus, to define the search space, we set the lower and upper bounds $-10 \leq \Re\{\epsilon_1\}, \Im\{\epsilon_1\}, \Re\{\epsilon_2\}, \Im\{\epsilon_2\} \leq 10$.

Our in-home implementations of the NE and EL, $(\mu/\rho, \lambda)$ and $(\mu/\rho + \lambda)$, ES were tested for their relative success looking for the solution from two hundred different initial states. Also, for completeness, we searched for the parameters $\Re\{\epsilon_1\}, \Im\{\epsilon_1\}, \Re\{\epsilon_2\}$, and $\Im\{\epsilon_2\}$ employing our in-home implementation of the PSO. To make the comparison with the ES – $(\mu/\rho + \lambda)$ in an objective manner, we set the size of the swarm $\mu_{\mathrm{PSO}} = \mu + \lambda$, where μ and λ are previously established sizes of the initial and secondary population of the EL strategy. Furthermore, we considered the same number of iterations for the optimization loop, in this way, the fitness function was evaluated by the PSO the same number of times as the ES – $(\mu/\rho + \lambda)$. In Fig. 3 we show the target spectra for different incidence angles and for both polarization modes (lines), and their corresponding optimized spectra (markers) found using the three strategies: ES – $(\mu/\rho + \lambda)$, ES – $(\mu/\rho, \lambda)$, and PSO. Since all the optimized spectra completely overlap, only a single set of markers is shown for each curve.

In Figs. 4 and 5, we summarize the results obtained with the three inversion schemes. Each histogram represents the number of realizations for which the unknowns (real and imaginary parts of ϵ_1 and ϵ_2) fall within the established interval. For instance, in the case of $\Re\{\epsilon_1\}$, we only consider values that fall between 2.3 and 2.4. In both figures, panels (a) and (b) correspond to the ES – $(\mu/\rho, \lambda)$ strategy, (c) and (d) to the ES – $(\mu/\rho + \lambda)$ strategy, and (e) and (f) to the PSO. In each panel we include all the values retrieved, considering both polarization modes and the following four angles of incidence: 0°, 30°, 45°, and 60°. This means that we evaluated the target function considering seven different illumination conditions, as for normal incidence, the response is the same for both polarizations. We repeated each numerical experiment 200 times, making a total of 1400 realizations.

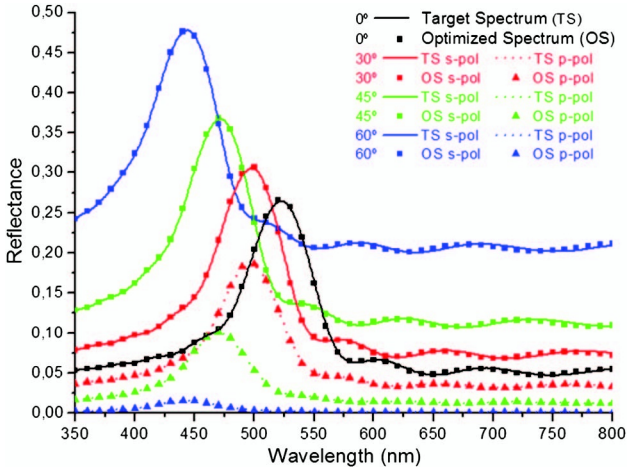

Fig. 3. Target and optimized reflectance spectra from a bilayer periodic structure with nine periods, layers' thicknesses $d_1 = 60$ nm, $d_2 = 100$ nm, and dielectric constants $\epsilon_1 = 2.3829 + i0.434$ and $\epsilon_2 = 2.8215 + i0.1008$, for different angles of incidence. The incidence medium is air and the dielectric constant of the substrate is $(\epsilon_1 + \epsilon_2)/2$.

Some typical results obtained by means of the three strategies are summarized in Table 1, where we show the percentage of relative success for each variable in the retrieval of the dielectric constants for the different strategies. In each percentage, we considered the retrieved values of the unknowns that fall within the established intervals, which in this case are [2.3, 2.4] and [0.42, 0.44] for the real and imaginary parts of ϵ_1, respectively, and [2.8, 2.9] and [0.1, 0.102] for the real and imaginary parts of ϵ_2, respectively. As mentioned before, a direct comparison between the ES and the PSO is not possible because of the different biological paradigms on which each technique is based. Nevertheless, putting aside that none of the global optimization methods reported in the literature can guarantee the convergence to the global optimum, the numerical results shown in Table 1 suggest the existence of what seems to be a unique solution. It is important to remark that in each histogram, we include the results of seven independent processes (two polarizations, four incidence angles, as explained above), and all the converged values of the unknown variables fall within a very narrow interval. These results are refreshing and provide some confidence in our approach, as any of

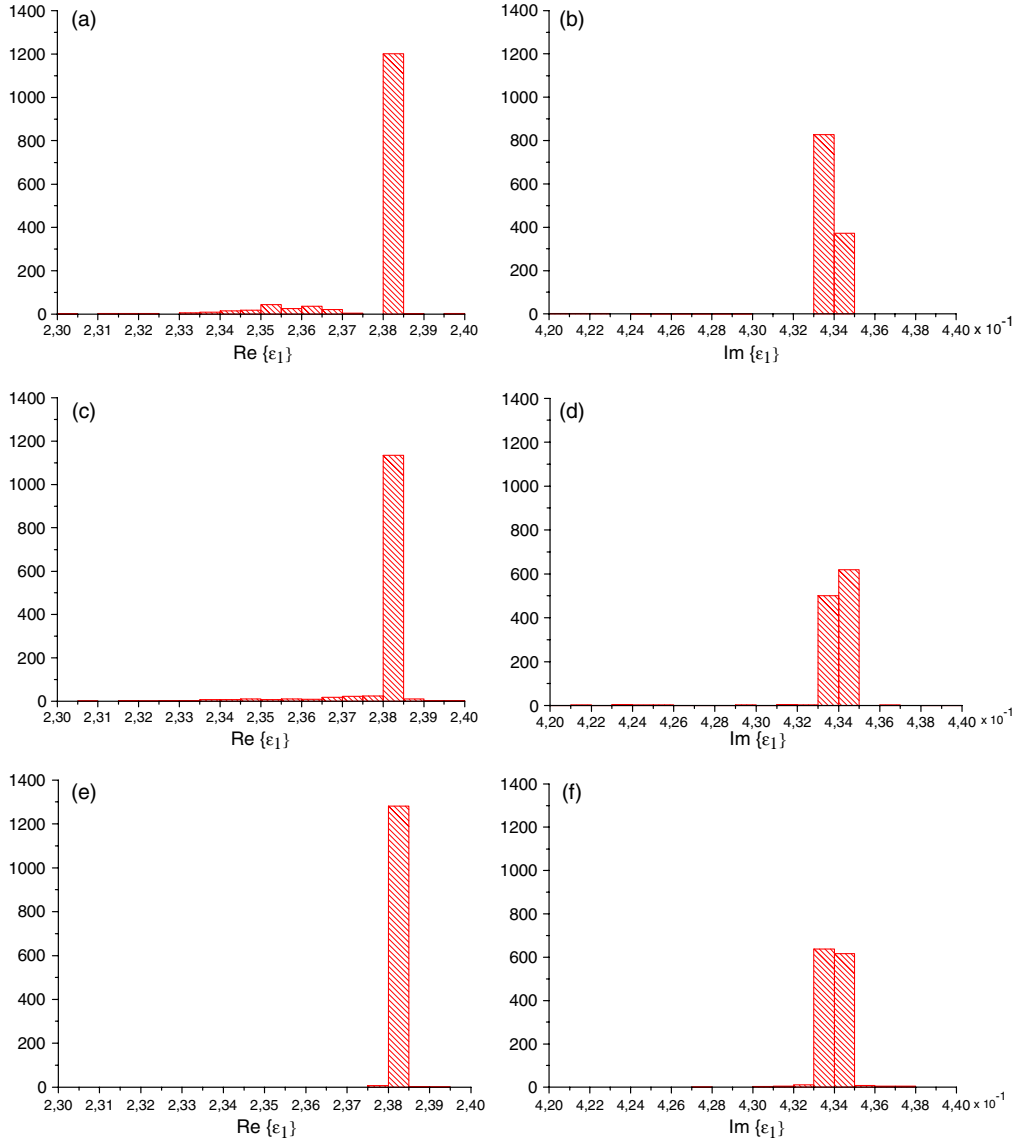

Fig. 4. Histograms of the retrieved values of the real and imaginary parts of ϵ_1 corresponding to the same structure of Fig. 2, for the three inversion schemes: (a)–(b) ES – $(\mu/\rho + \lambda)$; (c)–(d) ES – $(\mu/\rho, \lambda)$; (e)–(f) PSO. In each figure the converged results for both polarization modes and for the four incidence angles considered (0°, 30°, 45°, and 60°) are included.

the three strategies could be used to retrieve the unknown parameters throughout this work. However, at least for this first example, the EL strategy appears to be the less suitable option.

B. Application Example: The *Ceroglossus suturalis* Beetle

Ceroglossus suturalis beetles mostly live endemically in the forests of the Argentinean Patagonia and the south of Chili. They exhibit a characteristic iridescent coloration that can vary between yellow-green and brown-copper, as shown in Fig. 6(a). The structural arrangement that produces color in this species is a periodic multilayer composed of alternating layers of materials with different optical density, located in the epicuticle [36]. Scanning (SEM) and transmission electron microscopy (TEM) images of a transversal cut of the cuticle reveal a periodic multilayer system. Each period comprises two layers of different materials, as shown in Fig. 6(b). A total of nine periods was found in the analyzed sample, the layers' thicknesses being 100 and 60 nm. These values were obtained after an exhaustive study and analysis of several SEM and TEM images using the *ImageJ* software [37]. The parameter extraction was completed with a statistical analysis.

The specular reflectance spectrum of the elytron was measured using two optical fibers. One end of the first fiber was connected to a tungsten lamp, and the output beam was directed to the sample after being focused and linearly polarized. The light reflected by the sample was collected by the second fiber after passing through a Glan Thompson polarizer, and delivered to an Ocean Optics USB650 spectrometer. In Fig. 7 (solid line) we show the measured results for an incidence angle of 15° and for *s* polarization. To retrieve the complex dielectric

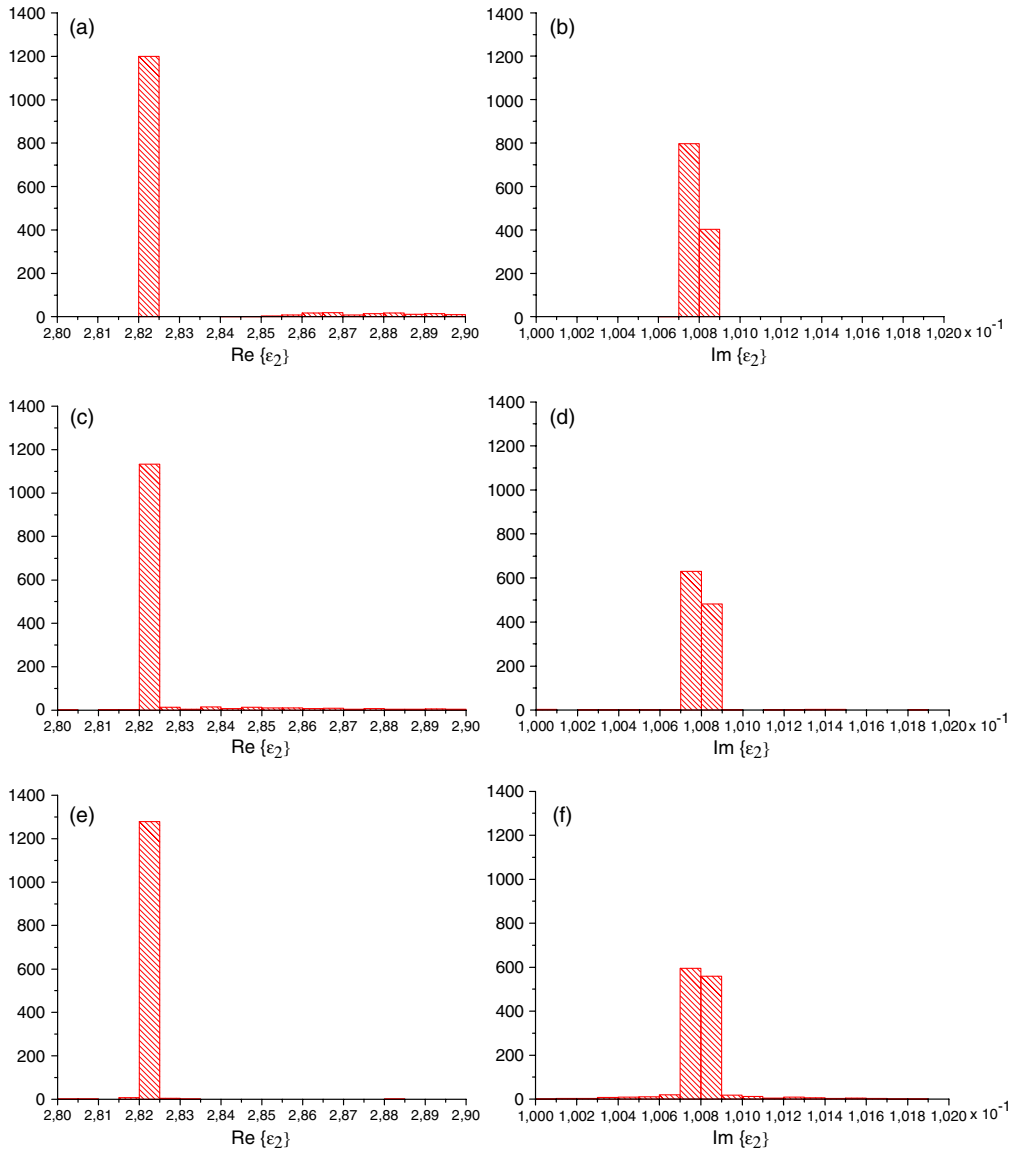

Fig. 5. Histograms of the retrieved values of the real and imaginary parts of ϵ_2 corresponding to the same structure of Fig. 4, for the three inversion schemes: (a)–(b) ES – $(\mu/\rho + \lambda)$; (c)–(d) ES – $(\mu/\rho, \lambda)$; (e)–(f) PSO. In each figure, the converged results for both polarization modes and for the four incidence angles considered (0°, 30°, 45°, and 60°) are included.

constants of the materials that comprise this natural system (the dielectric constant of the substrate is assumed to be the average of those of the individual layers), we assumed a perfectly periodic planar multilayer structure with known values of the layers' thicknesses (60 and 100 nm). The sizes of the initial and secondary populations of the ES, as well as that of PSO population, were the same as in the previous example. Also, we searched for the solution from 50 different initial states with the three optimization strategies. The number of generations was set to $g = 200$ and it provided the termination criterion.

Table 1. Relative Success (percentage) of the Different Strategies for the Retrieval of the Real and Imaginary Parts of the Dielectric Functions of Both Materials that Comprise the Multilayer System for the Numerically Generated Example

	$\Re\{\epsilon_1\}$	$\Im\{\epsilon_1\}$	$\Re\{\epsilon_2\}$	$\Im\{\epsilon_2\}$
NE	99.36	86.57	94.86	85.71
EL	91.07	82.36	89.93	80.50
PSO	92.29	92.07	92.57	90.21

In the search for the optimized solution by using the three strategies, we found two sets of values of ϵ_1 and ϵ_2, as shown in Table 2. These two sets appear with different frequencies in the solutions given by the different strategies, and also exhibit different values of the fitness function: ≈0.96 for set 1 and ≈1.2 for set 2. In Table 3, we show the occurrence rate (percentage) of set 1 and set 2, for each one of the three strategies. As observed, the relative success of the ES – $(\mu/\rho, \lambda)$ strategy for the retrieval of set 1 is significantly lower than that achieved by the ES – $(\mu/\rho + \lambda)$ and the PSO [notice there is a remaining

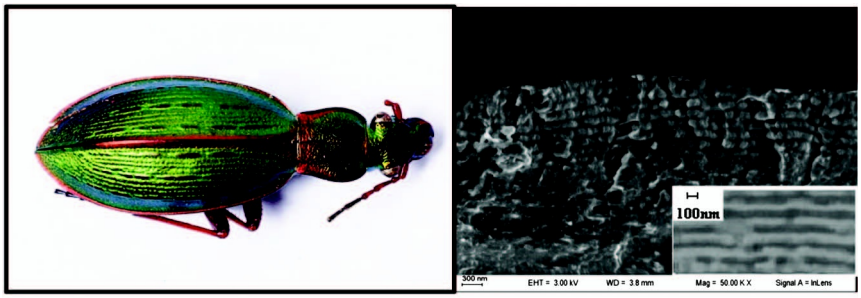

Fig. 6. (a) View of the dorsal side of a *Ceroglossus suturalis* specimen. (b) SEM image of a transversal cut of the cuticle. Inset: TEM image of the multilayer structure.

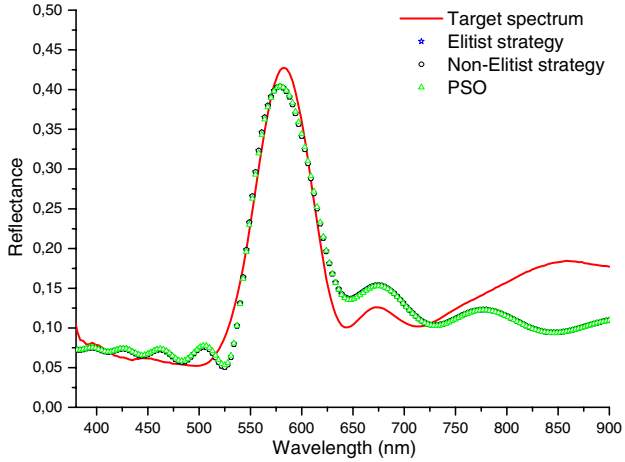

Fig. 7. Specular reflectance spectra of the *Ceroglossus suturalis* beetle for an incidence angle of 15° and *s* polarization. The red solid line corresponds to the experimental measurement; the blue stars, the black circles, and the green triangles correspond to the ES – $(\mu/\rho + \lambda)$, ES – $(\mu/\rho, \lambda)$ strategies and PSO, respectively.

percentage of solutions given by the ES – $(\mu/\rho, \lambda)$ (26%) that is not included in the table since they give extremely large values of the fitness function]. Set 1 has the lowest fitness achieved, and then it appears as the best candidate for the global optimum that we are looking for. On the other hand, since the fitness value for set 2 is higher than that of set 1, it seems to correspond to a local optimum, and should be discarded. Physically, the retrieved value of $\Re\{\epsilon_1\}$ in set 2 is higher than those corresponding to biological media, and then set 2 does not constitute an acceptable solution of the present problem. The performance of the ES – $(\mu/\rho + \lambda)$ and the PSO strategies seem to be very successful in the retrieval of the correct values of the dielectric constants. This fact suggests that elitism is the most adapted strategy

Table 2. Real and Imaginary Parts of the Retrieved Dielectric Functions of Both Materials that Comprise the Multilayer System in the *Ceroglossus suturalis* Beetle

	$\Re\{\epsilon_1\}$	$\Im\{\epsilon_1\}$	$\Re\{\epsilon_2\}$	$\Im\{\epsilon_2\}$
Set 1	2.85	0.008	3.530	0.24
Set 2	4.1	2.10^{-7}	2.138	0.39

Table 3. Percentage of Occurence of Each Solution for the Different Strategies

	NE	EL	PSO
Set 1	62	100	96
Set 2	12	0	4

in the present context. In Fig. 7, we compare the target experimental spectrum and the corresponding spectra generated with the parameters retrieved by each strategy. Since the values of the dielectric constants of set 1 are almost nearly the same for the three strategies, i.e., only differ in the third significant digit, the corresponding curves are completely overlapped. There is a very good agreement between the experimental and the retrieved optimized spectra. The main peak is very well reproduced both in spectral location as well as in reflectance value, and the overall features of the experimental curve are also satisfactorily described by the optimized reflectance. Although the dielectric constant values of the materials comprising the *Ceroglossus suturalis* multilayer are unknown, the retrieved values of their real and imaginary parts lie within the range of values that are widespread in nature [3]. However, to ensure the uniqueness of the solution and the convergence to the actual values of the dielectric constants, reflectance measurements for several angles of incidence, as well as for *p*- and *s*- polarization states, should be simultaneously included in the fitness function.

C. Discussion

The results of the last example show that heuristic optimization techniques constitute a powerful tool to retrieve, from experimental reflectance data, the dielectric constant of biological tissues. However, there are several aspects that have to be taken into account when applying these tools to obtain the values of not precisely known parameters in biological structures.

Photonic structures found in nature are essentially complex and three-dimensional. In the particular case of Coleoptera, the cuticle, the complex system of various layers, is at the origin of the numerous optical phenomena resulting in the physical colors of these beings [3]. Even these multilayer structures,

which appear to be among the simplest photonic structures found in nature, are very difficult to characterize, not only due to the highly precise cuts that must precede the electron microscopy images, for instance, the layers' thicknesses are altered if the cut is not perfectly perpendicular to the top surface, but also due to the variation of the structure in different samples or even in different sections of the same sample. Although average parameters, such as the layers' thicknesses, can be estimated from different images, we cannot guarantee the parameters of the measured sample.

Another important aspect that must be taken into account is the capability of the proposed model, usually ideal in one or more aspects, to reproduce the response of the natural system under study. In multilayer structures, for instance, the perfect periodicity imposed by the model or the abrupt change in the refractive index of adjacent layers might result in the failure of the optimization techniques to find a successful solution, which implies the impossibility of finding reasonable values for the dielectric constants. Also, it has to be mentioned that the experimental reflectance measurements of biological structures can suffer from additional error sources originated in characteristics of the sample, such as the curvature and the roughness, which might significantly affect the measured values.

4. Conclusion

We have proposed a heuristic inversion tool to retrieve some relevant parameters of natural photonic structures. We considered a multilayer periodic structure and investigated and compared the performance of three different optimization strategies for the retrieval of the refractive indices of the constituent materials. As an application example, we investigated the *Ceroglossus suturalis* beetle, which exhibits an iridescent coloration produced by the interaction of light with the multilayer structure present in its epicuticle. It was shown that the two different bio-inspired techniques explored in this paper, i.e, ES (mainly the EL one) and the PSO, provide good estimates of the real and imaginary parts of the dielectric constants of the layers' materials. It is noteworthy to mention that nowadays, the actual values are not yet precisely known. Also, it is important to remark that the choice of the illustrative examples presented in this work is not restrictive and the relevant parameters of different and more complex biological structures could be equally retrieved if an appropriate model is used.

Despite the promising results obtained, there are still different aspects of the inversion schemes proposed that must be improved to guarantee, in all cases, the uniqueness of the solution and the convergence to what could be thought of as the global optimum. One way to constrain the search space would be to simultaneously include, in the fitness function, the information of several angles of incidence, as well as that of the *p*- and *s*-polarization states. Moreover, a local optimizer could be employed to refine the solution found by the ES and the PSO. However, the iterative nature of these strategies would certainly lead to another important issue that must be taken into account: the performance of each strategy with respect to the computing time, as the number of realizations and generations should be adapted to minimize the time required to converge to the right solution. One possible way to bypass this situation, although further work is still required, is to employ fitness prediction, a hybrid technique that makes use of neural networks to predict the fitness value and to avoid costly evaluations with the electromagnetic model.

Work is already in progress toward an approach that should make the model more realistic and useful for the retrieval of the relevant parameters of biological structures. It consists in the inclusion, within the optimization loop, of a Debye's or a Cole–Cole model to describe the frequency-dependent dielectric permittivity of the layers' materials. The goal in this case is not to obtain the dielectric function directly from the spectrum but, instead, to optimize the parameters of the dielectric function's model. Also, it is well known that many biological tissues exhibit anisotropic properties, and then the inclusion of more general constitutive relations for the materials involved would constitute a valuable contribution for the knowledge of the optical properties of natural materials.

D. S., A. L., and M. I. acknowledge partial support from Consejo Nacional de Investigaciones Cientficas y Técnicas (CONICET PIP 112-200801-01880) and Universidad de Buenos Aires (UBA-20020100100533). A. V. and D. M. gratefully acknowledge Dr. C.-A. Duhamel for fruitful discussions concerning the performance of the ES and PSO techniques.

References

1. A. Parker, "515 million years of structural colour," J. Opt. A **2**, R15–R28 (2000).
2. P. Vukusic and J. R. Sambles, "Photonic structures in biology," Nature **424**, 852–855 (2003).
3. S. Berthier, *Iridescences, the Physical Colours of Insects* (Springer Science+Business Media, LLC, 2007).
4. S. Kinoshita, *Structural Colors in the Realm of Nature* (World Scientific, 2008).
5. H. M. Fox and G. Vevers, *The Nature of Animal Colours* (Sidgwick and Jackson, 1960).
6. P. Vukusic and D. G. Stavenga, "Physical methods for investigating structural colours in biological systems," J. R. Soc. Interface **6**, S133–S148 (2009).
7. S. Berthier, E. Charron, and A. Da Silva, "Determination of the cuticle index of the scales of the iridescent butterfly Morpho menelaus," Opt. Commun. **228**, 349–356 (2003).
8. P. Vukusic, J. R. Sambles, C. R. Lawrence, and R. J. Wootton, "Quantified interference and diffraction in single *Morpho* butterfly scales," Proc. R. Soc. Lond. B **266**, 1403–1411 (1999).
9. H. L. Leertouwer, B. D. Wilts, and D. G. Stavenga, "Refractive index and dispersion of butterfly chitin and bird keratin measured by polarizing interference microscopy," Opt. Express **19**, 24061–24066 (2011).

10. J. A. Noyes, P. Vukusic, and I. R. Hooper, "Experimental method for reliably establishing the refractive index of buprestid beetle exocuticle," Opt. Express **15**, 4351–4357 (2007).
11. S. Yoshioka and S. Kinoshita, "Direct determination of the refractive index of natural multilayer systems," Phys. Rev. E **83**, 051917 (2011).
12. H. Arwin, R. Magnusson, J. Landin, and K. Jarrendahl, "Chirality-induced polarization effects in the cuticle of scarab beetles: 100 years after Michelson," Philos. Mag. **92** (12), 1583–1599 (2012).
13. S. Berthier, J. Boulenguez, and Z. Bálint, "Multiscaled polarization effects in *Suneve coronata* (Lepidoptera) and other insects: application to anti-counterfeiting of banknotes," App. Phys. A **86**, 123–130 (2007).
14. D. Macías, A. Vial, and D. Barchiesi, "Application of evolution strategies for the solution of an inverse problem in near-field optics," J. Opt. Soc. Am. A **21**, 1465–1471 (2004).
15. D. Macías, G. Olague, and E. R. Méndez, "Inverse scattering with far-field intensity data: random surfaces that belong to a well-defined statistical class," Waves Random Complex Media **16**, 545–560 (2006).
16. A. B. Djurišic, J. M. Elazar, and A. D. Rakic, "Modeling the optical constants of solids using acceptance-probability-controlled simulated annealing with adaptive move generation procedure," Phys. Rev. E **55**, 4797–4803 (1997).
17. A. Vial, A. S. Grimault, D. Macías, D. Barchiesi, and M. Lamy de la Chapelle, "Improved analytical fit of gold dispersion: application to the modelling of extinction spectra with the FDTD method," Phys. Rev. B **71**, 085416 (2005).
18. D. Macías and A. Vial, "Optimal design of plasmonic nanostructures for plasmon-interference assisted lithography," Appl. Phys. B **93**, 159–163 (2008).
19. D. Barchiesi, D. Macas, L. Belmar-Letellier, D. van Labeke, M. Lamy de la Chapelle, T. Toury, E. Kremer, L. Moreau, and T. Grosges, "Plasmonics: influence of the intermediate (or stick) layer on the efficiency of sensors," Appl. Phys. B **93**, 177–181 (2008).
20. A. Tassadit, D. Macías, J. A. Sánchez-Gil, P.-M. Adam, and R. Rodriguez-Oliveros, "Metal nanostars: Stochastic optimization of resonant scattering properties," Superlattices Microstruct. **49**, 288–293 (2011).
21. D. Macías, P.-M. Adam, V. Ruiz-Cortés, R. Rodríguez-Oliveros, and J. A. Sánchez-Gil, "Heuristic optimization for the design of plasmonic nanowires with specific resonant and scattering properties," Opt. Express **20**, 13146–13163 (2012).
22. K. R. Thomas, M. Kolle, H. M. Whitney, B. J. Glover, and U. Steiner, "Function of blue iridescence in tropical understorey plants," J. R. Soc. Interface **7**, 1699–1707 (2010).
23. M. F. Land, J. Horwood, M. L. M. Lim, and D. Li, "Optics of the ultraviolet reflecting scales of a jumping spider," Proc. R. Soc. B **274**, 1583–1589 (2007).
24. T. D. Schultz and M. A. Rankin, "The ultrastructure of the epicuticular interference reflectors of tiger beetles (*Cicindela*)," J. Exp. Biol. **117**, 87–110 (1985).
25. K. Miyamoto and A. Kosaku, "Cuticular microstructures and their relationship to structural color in the Shieldbug *Poecilocoris lewisi* distant," Forma **17**, 155–167 (2002).
26. J. P. Vigneron, M. Rassart, C. Vandenbem, V. Lousse, O. Deparis, L. P. Birø, D. Dedouaire, A. Cornet, and P. Defrance, "Spectral filtering of visible light by the cuticle of metallic woodboring beetles and microfabrication of a matching bioinspired material," Phys. Rev. E **73**, 041905 (2006).
27. A. E. Seago, P. Brady, J.-P. Vigneron, and T. D. Schultz, "Gold bugs and beyond: a review of iridescence and structural colour mechanisms in beetles (Coleoptera)," J. R. Soc. Interface **6**, S165–S184 (2009).
28. D. G. Stavenga, B. D. Wilts, H. L. Leertouwer, and T. Hariyama, "Polarized iridescence of the multilayered elytra of the Japanese jewel beetle, *Chrysochroa fulgidissima*," Philos. Trans. R. Soc. Biol. Sci. **366**, 709–723 (2011).
29. H. G. Beyer, *The Theory of Evolution Strategies* (Springer, 2001).
30. R. C. Eberhart and J. Kennedy, "A new optimizer using particle swarm theory," in *Proceedings of the Sixth International Symposium on Micro Machine and Human Science* (IEEE, 1995), pp. 39–43.
31. J. H. Holland, *Adaptation in Natural and Artificial Systems* (University of Michigan, 1975).
32. H.-P. Schwefel, *Evolution and Optimum Seeking* (Wiley-Interscience, 1995).
33. J. Robinson and Y. Rahmat-Samii, "Particle swarm optimization in electromagnetics," IEEE Trans. Antennas Propag. **52**, 397–407 (2004).
34. R. Poli, J. Kennedy, and T. Blackwell, "Particle swarm optimization: an overview," Swarm Intell. **1**, 33–57 (2007).
35. P. Yeh and A. Yariv, *Optical Waves in Crystals* (Wiley, 1984).
36. A. Luna, D. Skigin, M. Inchaussandague, and A. Roig Alsina, "Structural color in beetles of South America," Proc. SPIE **7782**, 778205 (2010).
37. ImageJ is a public domain, Java-based image processing program, http://rsbweb.nih.gov/ij/.